BMP signaling maintains auricular chondrocyte identity and prevents microtia development by inhibiting protein kinase A

Ruichen Yang[1*], Hongshang Chu[1*], Hua Yue[2], Yuji Mishina[3], Zhenlin Zhang[2], Huijuan Liu[1,5], and Baojie Li[1,4,5]

[1]Bio-X Institutes, Key Laboratory for the Genetics of Developmental and Neuropsychiatric Disorders, Ministry of Education, Shanghai Jiao Tong University, Shanghai, China.

[2]Department of Osteoporosis and Bone Diseases, Shanghai Clinical Research Center of Bone Disease, Shanghai Jiao Tong University Affiliated Sixth People's Hospital, Shanghai, China.

[3]Department of Biologic and Materials & Prosthodontics, University of Michigan School of Dentistry, Ann Arbor, MI, United States.

[4]Institute of Traditional Chinese Medicine and Stem Cell Research, Chengdu University of Traditional Chinese Medicine, Chengdu, China.

* equal contribution

[5] Correspondence:
Baojie Li: libj@sjtu.edu.cn

Or

Huijuan Liu liuhj@sjtu.edu.cn

Abstract

Elastic cartilage constitutes a major component of the external ear, which functions to guide sound to the middle and inner ears. Defects in auricle development cause congenital microtia, which affects hearing and appearance in patients. Mutations in several genes have been implicated in microtia development, yet, the pathogenesis of this disorder remains incompletely understood. Here, we show that *Prrx1* genetically marks auricular chondrocytes in adult mice. Interestingly, BMP-Smad1/5/9 signaling in chondrocytes is increasingly activated from the proximal to distal segments of the ear, which is associated with a decrease in chondrocyte regenerative activity. Ablation of *Bmpr1a* in auricular chondrocytes led to chondrocyte atrophy and microtia development at the distal part. Transcriptome analysis revealed that *Bmpr1a* deficiency caused a switch from the chondrogenic program to the osteogenic program, accompanied by enhanced protein kinase A activation, likely through increased expression of *Adcy5/8*. Inhibition of PKA blocked chondrocyte-to-osteoblast transformation and microtia development. Moreover, analysis of single-cell RNA-seq of human microtia samples uncovered enriched gene expression in the PKA pathway and chondrocyte-to-osteoblast transformation process. These findings suggest that auricle cartilage is actively maintained by BMP signaling, which maintains chondrocyte identity by suppressing osteogenic differentiation.

Introduction

The ear is an organ of hearing and equilibrium. The external ear (auricle), which contains many curves and folds, functions to collect and funnel sound waves into the middle and inner ear (Anthwal and Thompson, 2016; Fuchs and Tucker, 2015). The major component of the ear is elastic cartilage, a connective tissue composed of type II collagen, proteoglycans and glycosaminoglycans (Bielajew et al., 2020; Chen et al., 2021). Defects in auricle development can lead to microtia, a congenital disease characterized by deformed or underdeveloped ears that affects 0.83-4.34 per 10000 births (Gendron et al., 2016; Lu et al., 2020). Microtia causes hearing problems and delays in language learning (Gendron et al., 2016). Genetic studies have shown that microtia is linked to mutations in *ROBO1/ROBO2*, *HOXA2*, *SIX*, *TBX1*, or *CHUK* in humans (Cox et al., 2014; Huang et al., 2023; Lu et al., 2020; Quiat et al., 2022). In mice, Prrx1 and Prrx2, FGF, BMP, and Wnt have been shown to affect auricle development (ten Berge et al., 1998; Xie et al., 2020). However, the molecular etiology of microtia remains incompletely understood. Currently, microtia is treated with ear reconstruction (Evenbratt et al., 2022; Kobayashi et al., 2011; Nordberg et al., 2022).

Cartilage is an avascular and slow-turnover tissue that receives nutrients and external signals via diffusion (DiDomenico et al., 2018). In addition to elastic cartilage, hyaline cartilage and fibrocartilage are found in mammals. Cartilage is located in different parts of the body and has several important functions, including support, protection, and cushioning (Bielajew et al., 2020; Liu et al., 2017). Elastic cartilage is found in the ear, epiglottis, nose, and trachea, and its main function is to provide strength and elasticity to the organs. All cartilages are formed and maintained solely by chondrocytes (Kozhemyakina et al., 2015). Chondrocytes are extensively studied in endochondral ossification, which forms long bones. Bone development starts with condensation of mesenchymal cells, which differentiate into chondrocytes and form a cartilage template for the bones. After proliferation, differentiation, and hypertrophic growth, hypertrophic chondrocytes undergo transformation into osteoblast/osteoprogenitors (transdifferentiation or dedifferentiation followed by

68 redifferentiation), forming bone (Jing et al., 2017; Mizuhashi et al., 2018; Newton et
69 al., 2019; Yang et al., 2014a; Yang et al., 2014b). On the other hand, auricle
70 chondrocytes are derived from pharyngeal arches 1 and 2 during development (Ritter
71 and Martin, 2019). Although the auricle contains $CD44^{+}CD90^{+}$ stem cells in the
72 perichondrium (Kobayashi et al., 2011), it has limited regenerative capacity even in
73 early postnatal mice (Abarca-Buis and Krotzsch, 2023).

74 Chondrocyte proliferation, differentiation, and hypertrophy are regulated by BMPs,
75 FGFs, IHHs, PTHrp, and Wnts. In particular, BMP signaling positively regulates the
76 initiation and differentiation of chondrocytes (Murtaugh et al., 1999; Thielen et al.,
77 2019; Ueharu and Mishina, 2023). BMPs are members of the TGFβ superfamily, which
78 bind to BMP receptor IA and IB and activate Smad1/5/9, which, together with Smad4,
79 enter the nucleus to affect gene expression. *Bmpr1a* and *1b* double knockout mice have
80 no chondrocyte formation (Yoon et al., 2005). Moreover, ablation of *Smad1* or *Smad5*
81 in chondrocytes leads to severe chondrodysplasia (Retting et al., 2009), indicating that
82 BMP signaling is essential for maintenance of the chondrogenic differentiation program.
83 In addition, chondrocyte-specific knockout of *Bmpr1a* and *Bmpr1b* resulted in defects
84 in the terminal differentiation of chondrocytes (Yoon et al., 2006). BMPs induce
85 chondrocyte differentiation by controlling the expression of Sox9, which initiates and
86 maintains the chondrocyte phenotype but inhibits chondrocyte hypertrophy (Akiyama
87 et al., 2002). Sox9 may interact with Runx2 and β-catenin to regulate chondrocyte
88 differentiation and hypertrophy (Kozhemyakina et al., 2015; Takarada et al., 2013). A
89 recent study showed that *Sox9* is required to prevent growth plate closure postnatally,
90 with Sox9 ablation leading to transformation from chondrocytes to osteoprogenitor
91 cells (Haseeb et al., 2021).

92 While previous studies have uncovered essential roles for BMP signaling in
93 chondrogenic differentiation during skeletal development, it remains unclear whether
94 BMP signaling plays a role in cartilage maintenance in adult mice. Organ maintenance
95 is an important process since it accounts for 90% of the lifetime of mice. Here, we
96 provide genetic evidence that BMP signaling maintains the cell fate of auricle

chondrocytes. In the absence of BMP signaling, chondrocytes become osteogenic progenitors with reduced volume, leading to shrinkage of the distal auricle and morphological changes that resemble microtia. This study uncovered a new function for BMP signaling and improved our understanding of the pathogenesis of microtia.

Results

Prrx1 marks auricle chondrocytes but few epiphyseal or articular chondrocytes

We have recently shown that *Prrx1* marks $CD31^{-}CD45^{-}CD130^{+}CD200^{+}CD51^{+}$ skeletal stem cells that are required for bone maintenance in adult mice (Liu et al., 2022). Our lineage tracing experiments showed that *Prrx1* marked all chondrocytes in the auricle (Figure 1A). This finding is in contrast to the labeling of very small populations of chondrocytes in the growth plates and articular cartilages (Figure 1B). As expected, *Prrx1* also marked dermal cells in the skin of the ear in adult mice (Figure 1A); we previously showed that *Prrx1* marks $CD31^{-}CD45^{-}CD200^{+}CD51^{+}$ dermal stem cells (Liu et al., 2022). Immunostaining results showed that auricle chondrocytes did not express Vimentin or Col1α1/2, which were mainly expressed in the dermis of the ear, or Col2 or Col10 (Figure 1C and data not shown). Moreover, αSMA is mainly expressed in the smooth muscle of blood vessels (Figure 1C). These results suggest a difference between auricle cartilage and articular cartilage and growth plates.

We also traced *Prrx1* lineage cells in *Prrx1-CreERT; R26*^{tdTomato} mice that received TAM at E8.5, E13.5, or p21. We found that auricle chondrocytes were $Tomato^{+}$ under these conditions even only one dose of TAM (1/10 of the dose for adult mice) was given to the pregnant mice at E8.5 or E13.5 (Figure 1-figure supplement 1). However, while E8.5 mice showed $Tomato^{+}$ chondrocytes at both articular cartilage and growth plate, E13.5 or p21 mice showed much fewer $Tomato^{+}$ chondrocytes at articular cartilage and growth plate (Figure 1-figure supplement 1). These results indicate that *Prrx1* expression differs in cartilages during development, growth, and maintenance.

Ablation of *Bmpr1a* in *Prrx1*$^{+}$ cells in adult mice led to microtia

We generated *Prrx1-CreERT; Bmpr1a*$^{f/f}$ mice to study the function of BMP signaling in adult cartilage. TAM was injected at 12 weeks of age. We observed a decrease in p-Smad1/5/9 on the ear sections of the *Prrx1-CreERT; Bmpr1a*$^{f/f}$ mice 60 days after TAM administration while the protein levels were not affected (Figure 2A and Figure 2-figure supplement 1A). qPCR analysis confirmed the ablation of *Bmpr1a* in the auricle cartilage (Figure 2B). Note that the size and body weight of *Prrx1-CreERT; Bmpr1a*$^{f/f}$ mice were slightly reduced (Figure 2-figure supplement 1B). Interestingly, the mice showed a quick decrease in the size of the external ear (Figure 2C), indicating a problem with auricle cartilage, which provides strength for the ear.

Histological analysis showed that the phenotype mainly occurred at the distal part

of the ear. The thickness of the cartilage was slightly reduced, associated with a great reduction in the cell size (Figure 2D). Staining for Ki67 showed that there was no difference in the number of proliferating cells between the mutant and control mice (Figure 2-figure supplement 1C). Note that there were very few proliferating cells in the mutant or control mice. Staining for apoptotic cells indicated that chondrocytes did not undergo apoptosis (Figure 2-figure supplement 1D). Overall, these results suggest that the ear phenotype observed in *Prrx1-CreERT; Bmpr1a*$^{f/f}$ mice is not due to decreases in the number of chondrocytes via altered proliferation and/or apoptosis; rather, it occurs through shrinkage of chondrocytes. Interestingly, deletion of *Prrx1* and its paralog gene *Prrx2* led to microtia development, while deletion of *Prrx1* leads to low-set ears and deletion of *Prrx2* does not affect ear development (Martin et al., 1995; ten Berge et al., 1998). These results suggest that these two genes play a redundant role in external ear development. However, we found no ear phenotype in *Prrx1-CreERT* (with one *Prrx1* allele deleted) or *Bmpr1a*$^{f/f}$ mice compared to wild-type mice (Figure 2-figure supplement 2A-C), suggesting that ablation of one copy of *Prrx1* does not affect ear maintenance.

The growth plate and the articular cartilage appeared to be normal in *Prrx1-CreERT; Bmpr1a*$^{f/f}$ mice (Figure 2-figure supplement 3A and 3B), likely due to the lack of labeling of chondrocytes at these locations. Moreover, Smad1/5/9 is reportedly activated in proliferating chondrocytes but not hypertrophic chondrocytes in the growth plate (Retting et al., 2009; Yoon et al., 2006).

Chondrocytes in the distal auricle have the weakest regenerative ability

A surprising finding is that the auricle phenotype mainly occurred in the distal part (Figures 2D), suggesting that there exists a cellular difference along the proximal–distal axis. Our immunostaining of p-Smad1/5/9 results revealed that BMP-Smad1/5/9 signaling is more active at the distal part than at the proximal or middle part, in young or old mice (Figure 2A and Figure 2-figure supplement 4A). We also harvested cartilage from the proximal, mid, and distal (1/3 each) parts of normal adult mice and performed western blotting. We found that BMP-Smad1/5/9 signaling was activated to a greater extent at the distal part of the auricle (Figure 2-figure supplement 4B). We then tested the regenerative potential of the proximal, mid, and distal parts of the auricle by performing cartilage regeneration assays. We generated a 0.2 cm hole at these three

166 locations and waited for 4 weeks. It was clear that the injury at the distal or middle part
167 could not be repaired, while the injury at the proximal part was repaired (Figure 2-figure
168 supplement 4C and 4D). These results suggest that chondrocytes at the distal part of the
169 auricle have the lowest regenerative activity and thus may be the most differentiated,
170 which is associated with the strongest activation of BMP-Smad1/5/9 signaling.

171 **Ablation of *Bmpr1a* in dermal cells did not cause microtia**

172 Since *Prrx1* also marks dermal cells in the ear, we could not exclude the possibility
173 that *Bmpr1a* ablation in dermal cells contributes to the ear phenotype. We found that
174 *Col1a2* marked dermal cells but not auricle chondrocytes in *Col1a2-CreERT;*
175 *R26*^{tdTomato} mice (Figure 2-figure supplement 5A). We generated *Col1a2-CreERT;*
176 *Bmpr1a*$^{f/f}$ mice by crossing *Col1a2-CreERT* mice and *Bmpr1a* floxed mice.
177 Immunostaining results showed that the levels of p-Smad1/5/9 in the dermis were
178 greatly reduced in dermal cells in the mutant mice (Figure 2-figure supplement 5B).
179 qPCR analysis confirmed the ablation of *Bmpr1a* in the dermal cells (Figure 2-figure
180 supplement 5C). The ears appeared normal in *Col1a2-CreERT; Bmpr1a*$^{f/f}$ mice 6
181 months after TAM injection (Figure 2-figure supplement 5D and 5E).

182 In addition, we traced the Acta2 (encoding αSMA) lineage cells in auricles and
183 found that Acta2 could mark a small portion of chondrocytes in the middle segment of
184 the auricle and smooth muscle cells of the blood vessels (Figure 2-figure supplement
185 6A). We also generated *Acta2-CreERT; Bmpr1a*$^{f/f}$ mice and found that ablation of
186 *Bmpr1a* in *Acta2*$^{+}$ cells did not produce an ear phenotype (Figure 2-figure supplement
187 6B-6E). These findings suggest that BMP-Smad1/5/9 signaling affects ear maintenance
188 via its effect on chondrocytes at the distal segment, with little contribution from dermal
189 cells or smooth muscle cells.

190 **Ablation of *Bmpr1a* in *Prrx1*$^{+}$ cells in young mice also led to microtia**

191 We then tested the effect of *Bmpr1a* ablation on *Prrx1*$^{+}$ cells in young mice. Three
192 doses of TAM were administered to P21 *Prrx1-CreERT; Bmpr1a*$^{f/f}$ mice, which were
193 sacrificed at the age of 2 months (Figure 3A). We observed a decrease in p-Smad1/5/9
194 on the ear sections of the *Prrx1-CreERT; Bmpr1a*$^{f/f}$ mice (Figure 3A). qPCR analysis
195 confirmed the ablation of *Bmpr1a* in the auricle cartilage (Figure 3B). We found
196 decreases in the ear size and the volumes of chondrocytes at the distal part of the ear in
197 *Prrx1-CreERT; Bmpr1a*$^{f/f}$ mice (Figure 3C and 3D). However, these mice showed
198 normal growth plates and articular cartilage (Figure 3-figure supplement 1A and 1B),

likely attributable to the lack of labeling of chondrocytes in the growth plate and articular cartilage in *Prrx1-CreERT; R26*^{tdTomato} mice (Figure 1-figure supplement 1). Overall, these results suggest that BMP signaling is required for both growth and maintenance of the auricle.

Alteration of transcription profiles in *Bmpr1a*-deficient chondrocytes

We then harvested the distal part of the auricle from three *Prrx1-CreERT; Bmpr1a*$^{f/f}$ and age- and gender-matched control mice. We prepared the total RNA and performed bulk RNA-seq. We found that the transcription of at least 500 genes was affected by *Bmpr1a* ablation (Figure 4A). KEGG and GO analyses revealed that *Bmpr1a* ablation led to increased expression of genes in inflammation, stemness, cell cycle, mesenchymal cell development, proximal/distal patterning, ear morphogenesis, wound healing, TGFβ signaling, and PKA signaling, whereas genes in chondrocyte differentiation, stem cell division, skeletal morphogenesis, extracellular matrix (ECM) genes, cartilage development, Hedgehog signaling, and Wnt signaling were suppressed (Figure 4B and 4C). These transcriptome results suggest that *Bmpr1a* ablation may cause chondrocyte-to-osteoblast transformation.

Further analysis showed that the expression of many ECM proteins was down-regulated in auricle cartilage of *Prrx1-CreERT; Bmpr1a*$^{f/f}$ mice (Figure 4-figure supplement 1A). Note that mRNA levels of Smad1/5/9 were unaltered in the auricle cartilage of the mutant mice (Figure 4-figure supplement 1B). Immunostaining revealed that the expression of Aggrecan and Col10 in the growth plates was unaltered in the mutant mice (Figure 4-figure supplement 1C), likely due to the lack of marking of growth plate chondrocytes by *Prrx1* in adult mice. Since ECM proteins are secreted by chondrocytes, we also checked the expression of proteins involved in protein trafficking and found that some were up-regulated and some were down-regulated (Figure 4-figure supplement 4D). The change in the expression of ECM and protein trafficking genes may reflect the shift from chondrocytes to osteoblasts and warrants further investigation. However, the expression of ER or Golgi stress-related genes, which play critical roles in chondrocyte differentiation and survival (Horigome et al., 2020; Wang et al., 2018), was not altered by *Bmpr1a* ablation (Figure 4-figure supplement 1E and 1F).

***Bmpr1a* deficiency leads to an auricle chondrocyte switch to osteoblasts**

The heatmaps of osteoblast-related and chondrocyte-related genes further support a chondrocyte-to-osteoblast transformation in the absence of BMP signaling (Figure 5A

232 and Figure 5-figure supplement 1A). To validate the above findings, we stained the
233 auricle for Col1α1, a marker for osteoblasts, and found that Col1α1 expression was
234 elevated in the auricle of the *Prrx1-CreERT; Bmpr1a*$^{f/f}$ mice compared to the control
235 mice (Figure 5B). We also stained for alkaline phosphatase (ALP), a marker for
236 osteoblasts, and found that ALP activity was greatly increased in the mutant mice
237 (Figure 5C). WB confirmed the increases in the expression of osteoblast marker Runx2
238 and osteocalcin (Figure 5D). These results suggest that in the absence of BMP signaling,
239 auricle chondrocytes transformed into osteoblasts/osteoprogenitors via
240 transdifferentiation or dedifferentiation/redifferentiation. Previous studies have shown
241 that Sox9 is involved in chondrocyte to osteoblast transformation (Lefebvre et al., 2019).
242 However, we found that Sox9 mRNA levels were not altered by *Bmpr1a* deficiency
243 (Figure 5-figure supplement 1B and 1C).

244 ***Bmpr1a* deficiency led to hyperactivation of the PKA pathway**

245 To understand the molecular mechanisms underlying the development of microtia,
246 we examined the signaling pathways altered by *Bmpr1a* deficiency in auricle samples.
247 We focused on the enhanced activation of the protein kinase A pathway, which is known
248 to regulate chondrocyte differentiation. PKA signaling has been shown to promote
249 chondrocyte differentiation but inhibit chondrocyte hypertrophy (Dy et al., 2012; Tsang
250 and Cheah, 2019). In addition, PKA-phosphorylated Sox9 (Huang et al., 2000) may
251 promote bone formation (Siddappa et al., 2008). Immunoassaying for p-Creb, a
252 substrate of PKA, suggests that PKA is activated in auricle chondrocytes compared to
253 the control counterparts (Figure 6A). Western blot analysis of the auricle samples
254 confirmed this finding (Figure 6B).

255 What caused the enhanced activation of the PKA pathway? Our RNA-seq data
256 showed that the expression of Adcy5 and Adcy8 enzymes responsible for cAMP
257 production, was upregulated in the *Bmpr1a*-deficient auricle samples. Our qPCR
258 analysis of auricle RNA showed that *Bmpr1a*-deficient auricle samples displayed
259 increases in *Adcy5* and *Adcy8* (Figure 6C).

260 **Inhibition of PKA signaling blocks microtia development in *Bmpr1a*-deficient**
261 **mice**

262 To demonstrate the function of elevated PKA signaling in the development of
263 microtia, we administered the PKA inhibitor H89 to *Prrx1-CreERT; Bmpr1a*$^{f/f}$ and
264 control mice immediately after TAM injection (Figure 7A). After 2 months, we found

that p-Creb was greatly suppressed and that the microtia phenotype was rescued in the mutant mice by H89, although the inhibitor did not affect the auricle in the normal mice (Figure 7B and 7C). Histological analysis revealed that chondrocyte atrophy and the decrease in ear size and cartilage thickness were rescued by H89 (Figure 7D). Staining results revealed that the levels of Col1α1 and the ALP activity returned to normal (Figure 7E and 7F). Western blot analysis of the auricle samples confirmed that inhibition of PKA rescued the abnormal Runx2 and osteocalcin expression (Figure 7G). Overall, these results suggest that elevated PKA signaling is responsible for microtia development and the transformation from chondrocytes to osteoblasts, consistent with the pro-osteogenic activity of PKA signaling.

Human microtia samples show increased PKA signaling and osteogenic differentiation

The above studies uncover a critical role for the BMP-PKA pathway in controlling auricle chondrocyte identity and microtia pathogenesis in mice. Literature search did not uncover any study on *Prrx1* in auricle chondrocytes in human. We also analyzed a single-cell RNA-seq dataset of the pinna of 2 microtia patients who may have disrupted *ROBO1/2* expression (Quiat et al., 2022) and detected a population of cells with osteoblast features besides chondrocytes, fibroblasts and endothelial cells (Figure 7-figure supplement 1A-D). Moreover, we found enriched gene expression in the PKA pathway, which was associated with *ADCY2* (Figure 7-figure supplement 1C-1E). These results suggest a chondrocyte-to-osteoblast transformation under the influence of the PKA pathway in microtia patient samples. Although recent studies have uncovered an interaction between the BMP pathway and the Robo pathway (Morita et al., 2023; Tumelty et al., 2018), the functional link between these pathways in chondrocytes awaits further investigation.

Discussion

Microtia is usually a congenital disorder that affects the hearing and psychological health of affected children. Many of the disease candidate genes are involved in the proliferation and differentiation of auricle chondrocytes and therefore the development or growth of auricle cartilage (Gendron et al., 2016; Huang et al., 2023). Here, we show that in young or adult mice, ablation of *Bmpr1a* in auricle chondrocytes, which are genetically labelled by *Prrx1*, leads to rapid development of microtia. The function of BMP signaling in mature auricle chondrocytes appears to maintain cell identity and prevent chondrocytes from transforming into osteoblasts/osteoprogenitors. These results suggest that auricle appearance and integrity are actively maintained by BMP signaling.

Our study thus uncovered a novel function of BMP signaling in addition to its critical roles in chondrocyte proliferation and differentiation during endochondral ossification (Thielen et al., 2019). Defects in BMP-Smad1/5/9 signaling lead to achondroplasia and skeletal developmental defects. On the other hand, studies of *Bmpr1a* ablation mice using *Col1-CreERT*, *Prrx1-CreERT*, or *Dmp1-Cre* lines suggest that BMP-Smad1/5/9 signaling plays a modest pro-differentiation role in osteogenic lineage cells. Instead, BMP signaling in osteogenic lineage cells regulates osteoclastogenesis by affecting the relative expression of RANKL and OPG (He et al., 2017; Lim et al., 2016; Omi et al., 2019; Zhang et al., 2020). Here, we show that BMP signaling is required to maintain the cell fate of auricle chondrocytes by preventing them from osteogenic differentiation, thus expanding the physiological roles of BMP signaling in skeletal development and maintenance (Thielen et al., 2019). Intriguingly, ablation of *Bmpr1a* in adult mice using a transgenic *Prrx1-CreERT* line did not produce an ear phenotype (Biswas et al., 2018). One explanation is that the transgenic *Prrx1-CreERT* labels too few auricle chondrocytes, as it has been for endosteal and periosteal osteoblasts in adult mice, compared to the knock-in *Prrx1-CreERT* line (Liu et al., 2022). The difference is likely caused by the fact that the transgenic *Prrx1-CreERT* was driven by a 2.3 kilobase promoter of *Prrx1* that was inserted into unknow location in the genome, although this needs to be verified in the future. Moreover, although we

show that *Prrx1* specifically marks auricle chondrocytes but not growth plate or articular chondrocytes in adult mice, its use in auricle cartilage studies as a genetic marker is complicated by the labelling of dermal cells in the external ear.

Interestingly, we show that activation of BMP-Smad1/5/9 signaling in the auricle is uneven, with the distal part displaying the strongest activation in young or old mice. Accordingly, ablation of *Bmpr1a* in auricular chondrocytes mainly causes atrophy of the distal part. One possible explanation is that the distal part contains the most mature chondrocytes with the weakest regenerative ability. If so, it may mirror the trans-differentiation of terminally differentiated hypertrophic chondrocytes in the growth plate to osteoblasts (Tsang and Cheah, 2019). BMPs may be provided by chondrocytes themselves or by neighboring dermal cells, which warrants further investigation.

Our study suggests that the crosstalk between the BMP and PKA pathways plays a role in maintaining auricle chondrocyte fate. In the absence of *Bmpr1a*, the fate of chondrocytes is switched into osteoblast/osteoprogenitors, which can be blocked by PKA inhibition. Previous studies have shown that pharmacological inhibition of PKA efficiently blocks chondrogenic differentiation (Kozhemyakina et al., 2015). On the other hand, Sox9 inhibits chondrocyte hypertrophy and promotes the cell fate switch to osteoblasts/osteoprogenitors (Dy et al., 2012; Tsang and Cheah, 2019). This finding is consistent with a previous study showing that PKA promotes osteoblastogenesis and bone formation (Siddappa et al., 2008). How does BMP signaling regulate PKA activation? We found that the link is likely to be Adcy5/8, adenylate cyclases, whose expression is upregulated in the absence of BMP signaling. BMP signaling has been shown to suppress the expression of hepcidin and Robo4 (Morita et al., 2023; Wang et al., 2017). Since the Smad1/5/9 binding site in the promoters is very short, it may collaborate with other transcription factors to activate the transcription of target genes. In addition, BMP activates noncanonical signaling pathways, including MAPKs. As such, the underlying mechanisms for BMP-regulated expression of hepcidin, Robo4, Adcy5, and Adcy8 await further investigation (Morita et al., 2023; Wang et al., 2017).

Our findings may help to understand the pathogenesis of microtia in humans. A recent study uncovered a minimal microtia locus that carries a polymorphic repeat

element, which may disrupt *ROBO1* and *ROBO2* gene expression in the auricle and be responsible for the high incidence of microtia in East Asian and Amerindian populations (Quiat et al., 2022). Analysis of the scRNA-seq data from microtia patients revealed that the microtia patient samples also showed enriched expression of osteoblast-related genes and the PKA pathway genes, suggesting that human microtia may share a pathogenesis similar to that in *Prrx1-CreERT; Bmpr1a*$^{f/f}$ mice, although this needs to be verified in the future.

In summary, this study shows that auricular chondrocytes can be genetically marked by Prrx1. Auricular chondrocytes, especially at the distal part of the ear, display BMP-Smd1/5/9 activation, which is required to maintain chondrocyte fate. In the absence of BMP signaling, transformation of auricular chondrocytes into osteoblasts/osteoprogenitor cells will occur, leading to microtia development. This study thus deepens our understanding of microtia pathogenesis and expands the physiological functions of BMP-PKA crosstalk.

Materials and methods

Experimental design

The study was designed to examine the physiological function of BMP signaling in the maintenance of auricle chondrocyte and to elucidate the underlying molecular mechanisms.

Mouse maintenance

The knock-in *Prrx1-CreERT*^{2} mouse line was generated by Shanghai Biomodel Organism Science & Technology Development Co., Ltd. In this study, heterozygous *Prrx1-CreERT*^{2} mice were used for lineage tracing or gene ablation. *Rosa-tdTomato, Acta2-CreERT*^{2}, and *Col1α2-CreERT*^{2} mice were purchased from the Jackson Laboratory (https://www.jax.org/cn/). *Bmpr1a*$^{f/f}$ mice were generated in Yuji Mishina's laboratory. Animal experiments were carried out in accordance with recommendations in the National Research Council Guide for Care and Use of Laboratory Animals and in comply with relevant ethical regulations for animal testing and research, with the protocols approved by the Institutional Animal Care and Use Committee of Shanghai, China (SYXK(SH)2011-0112). This study follows the project that "Studies on the mechanism of MSC self-renewal differentiation and regulation of related tissue stem cells", which was approved by Shanghai Jiao Tong University in 2015 and the approval number is A2015027. Male mice were used in this study. Mice were anesthetized using 40 mg kg^{-1} sodium pentobarbital by intraperitoneal injection or euthanized by carbon dioxide inhalation.

Drug administration

Tamoxifen (TAM) (Sigma) was dissolved in corn oil and administered peritoneally to mice at 120 mg kg^{-1} body weight daily for 3 days (for P21 or adult mice). For E8.5 or E13.5 embryos, 1/10 of the dose was injected to the mother mice just one time. For genetic tracing or gene ablation, mice were euthanized at different time points after tamoxifen.

For in vivo inhibition of PKA, H89 (Selleck Chemicals, USA) was dissolved in 5% DMSO, 40% PEG300, 5% Tween 80, and 50% ddH_2O at a final concentration of 1.05

393 mg/ml and was administered intraperitoneally every other day after tamoxifen injection.
394 The dosage of H89 was 10 mg/kg (in 200 μl) each time. Mice were treated for 2 months
395 and then euthanized.

396 **Auricle regenerative experiments**

397 To investigate the regenerating ability of different parts of the mouse auricle, we drilled
398 a 2 mm (in diameter) hole at the distal, middle, or proximal parts of adult mice with a
399 uniform aperture. The mice were euthanized 1 month later, and the ear was analyzed to
400 assess the healing of the puncture wounds.

401 **RNA isolation and quantitative PCR**

402 Chondrocyte differentiation was also assessed with quantitative PCR. Total RNA
403 was extracted from the elastic cartilage using TRIzol reagent (Invitrogen), which was
404 reverse transcribed using the PrimerScriptTM RT reagent Kit (TaKaRa, RR037A) to
405 obtain cDNA. Quantitative PCR was performed using the Roche Light Cycler 480II
406 Assay system (Roche). The levels of different mRNA species were calculated with the
407 delta-delta CT method and normalized to *Actb*. The primer sequences are: *Bmpr1a,*
408 sense: 5'- ATCCGATGGCTGGTTGTGCTCA-3'; antisense: 5'-
409 CCAAATCACGGTTGTAACGACCC-3'; *Adcy5*, sense: 5'-
410 TCGCAATGCCTACCTCAAGGAG-3'; antisense: 5'-
411 GCGGATTGTGTCCGATGGAGTT-3'; *Adcy8*, sense: 5'-
412 CTGCTCACAGAGACCATCTACG-3'; antisense: 5'-
413 CAGCAGTGATGCTTCCTTGGTC-3'; *Sox9*, sense: 5'-
414 AGTCCCAGCGAACGCACATCA-3'; antisense: 5'-
415 GTCGTATTGCGAGCGGGTGAT-3'; *Actb*, sense: 5'-
416 GGCTGTATTCCCCTCCATCG-3'; antisense: 5'-CCAGTTGGTAACAATGCC
417 ATGT-3'.

418 **Immunohistochemistry and immunofluorescence staining**

419 The harvested ear tissues were fixed in 4% (vol/vol) neutral buffered formalin for
420 24 hours or directly embedded in optimal cutting temperature compound (OCT) by
421 liquid nitrogen without fixation. The harvested bone tissues were fixed in 4% (vol/vol)

422 neutral buffered formalin for 24 hours and decalcified in neutral 10% (wt/vol) EDTA
423 solution for 1 month at room temperature on the oscillator. For paraffin sectioning, the
424 samples were dehydrated, cleared, and embedded in paraffin blocks sequentially. The
425 paraffin-embedded tissues were cut at 10 μm with a paraffin microtome, and the frozen-
426 embedded tissues were cut at 8 μm with a cryostat. The ear tissue sections were
427 incubated overnight with anti-phospho-Smad1/5/9 antibody (Millipore, AB3848-1,
428 rabbit), anti-Ki67 antibody (Abcam, ab15580, rabbit), anti-Vimentin antibody (Abcam,
429 ab92547, rabbit), anti-αSMA antibody (Abcam, ab5694, rabbit), anti-Col1α1 antibody
430 (Abcam, ab21286, rabbit), anti-Col1α2 antibody (Santa Cruz, sc-393573, mouse), anti-
431 Aggrecan antibody (Millipore, AB1031, rabbit), anti-Col10 antibody (Abcam,ab58632,
432 rabbit), or anti-phospho-CREB antibody (UPSTATE, 06-519, rabbit). The sections were
433 then incubated with goat anti-rabbit, mouse, or rat secondary antibodies conjugated
434 with Alexa Fluor 488 or 555 (Thermo Fisher Scientific). Slides were mounted with
435 antifade mounting medium and DAPI (Thermo Fisher Scientific). Images were taken
436 under an Olympus DP72 microscope (Olympus Microsystems).

437 **H/E staining, ALP staining, and TUNEL staining**

438 Paraffin sections were used for H/E staining and ALP staining with a commercial
439 staining kit (TaKaRa, TRACP & ALP double-stain kit, Cat# MK300), while frozen
440 sections were used for TUNEL staining with a kit (Roche, In Situ Cell Death Detection
441 Kit, Fluorescein, REF11684795910).

442 **Western blotting**

443 Western blotting was performed with standard procedures. Proteins were extracted
444 from the distal, mid, and proximal parts of the cartilage of the mouse ear using RIPA
445 lysis buffer with 1 mM PMSF, 1 mg/ml pepstatin, leupeptin, and aprotonin. Samples
446 were separated on 10% SDS–PAGE gels and transferred onto PVDF membranes
447 (Millipore). Membranes were blocked with 5% milk or 3% BSA for 1 hr and incubated
448 with specific antibodies overnight at 4 °C on a shaker. The primary antibodies included
449 anti-phospho-Smad1/5/9 antibody (Millipore, AB3848-1, rabbit), anti-Smad1 antibody
450 (CST, 9743, rabbit), anti-RUNX2 antibody (CST, 12556, rabbit), anti-Osteocalcin

antibody (Abcam, ab93876, rabbit), anti-β-Actin antibody (Santa Cruz, sc47778, mouse), anti-phospho-CREB antibody (UPSTATE, 06-519, rabbit), or anti-CREB antibody (UPSTATE, 05-676, rabbit). The secondary antibodies included anti-rabbit IgG, HRP-linked antibody (CST, 7074, rabbit) and anti-mouse IgG, HRP-linked antibody (CST, 7076, mouse). The WB bands were visualized using the FluoChem M system (ProteinSimple). To quantify the western blotting results, we measured the density of each band by Image J, which was normalized to the loading control of the sample.

RNA sequencing

The distal part of the auricle of the mouse ear was harvested from control or knockout mice (n = 3 per group), from which RNA was isolated. RNA-seq was conducted by BGI Genomics Co., Ltd with the Illumina system. For data processing, SOAP nuke (v1.5.2) was applied to filter reads and saved in FASTQ format. After quality control, clean reads were aligned to the reference mouse genome using Bowtie2 (v2.2.5) with default parameters. Gene expression levels were calculated and blasted with HISAT (v2.0.4) based on the Burrows–Wheeler transform and Ferragina-Manzini. Clean reads were then detected in terms of randomicity, coverage and degree of saturation. Statistically significant (adjusted p value ≤ 0.05) genes with large expression changes (fold change ≥ 1.5) were defined as differentially expressed genes. In pathway analysis and Gene Ontology (GO) analysis, all candidate genes were assorted according to official classification with the KEGG or GO annotation result, and phyper (a function of R) was performed for GO and pathway functional enrichment. Furthermore, GO analysis of the stage-specific gene signature was performed in the biological process category. The p value calculating formula was used based on previous studies (Ge et al., 2021), and the false discovery rate (FDR) was calculated for each p value with FDR ≤ 0.05 defined as significantly enriched.

Statistical analysis

All measurements were collected by two authors who were blinded to the allocations of the mice. Image-Pro Plus was used to measure elastic cartilage thickness,

cell volume, and ear size. GraphPad Prism 9.5.0 software was used to analyze and plot the ear thickness, cell volume, ear size, qPCR data, and immunofluorescence results. All quantitative data are presented as the means ± SD unless indicated otherwise. One-way ANOVA (and nonparametric or mixed) and two-way ANOVA (or mixed model) for multiple comparisons and unpaired two-tailed Student's t test were applied to evaluate the correlation data, and $p<0.05$ was considered statistically significant. We ensure that we have not set criteria and exclusions in this study. For each analysis, we reported the exact value of *n* in each experimental group.

Declarations

Acknowledgments

We thank Shoutao Qiu and Yuping Li for their technical assistance.

Funding

The work as supported by the National Key Research and Development Program of China (2018YFA0800803) and National Natural Science Foundation of China (92268101 and 32230045).

Availability of Data and Materials

The mouse auricle bulk RNA-seq data of *Prrx1-CreERT; Bmpr1a*$^{f/f}$ and control mice have been deposited into NCBI (GSE240126). Human scRNA-seq data of auricle samples (GSE202441) were analyzed. All other data generated or analyzed during this study are included in this published article and its additional files.

Author contributions

B. L., Z. Z., and H. L. designed the experiments, R. Y., H. C., and H. Y. performed the experiments, R. Y. and H. C. prepared the figures, Y. M. provided reagents, B. L., Z. Z., and H. L. wrote the paper. All authors read and approved the final manuscript

Declaration of interests

The authors declare no competing interests.

Data Availability

All data generated or analyzed in this study are included in this article, and are available from the corresponding author on request.

Reference

Abarca-Buis, R.F., and Krotzsch, E. (2023). Proximal ear hole injury heals by limited regeneration during the early postnatal phase in mice. J Anat *242*, 402-416.

Akiyama, H., Chaboissier, M.C., Martin, J.F., Schedl, A., and de Crombrugghe, B. (2002). The transcription factor Sox9 has essential roles in successive steps of the chondrocyte differentiation pathway and is required for expression of Sox5 and Sox6. Genes Dev *16*, 2813-2828.

Anthwal, N., and Thompson, H. (2016). The development of the mammalian outer and middle ear. J Anat *228*, 217-232.

Bielajew, B.J., Hu, J.C., and Athanasiou, K.A. (2020). Collagen: quantification, biomechanics, and role of minor subtypes in cartilage. Nat Rev Mater *5*, 730-747.

Biswas, S., Li, P., Wu, H.G., Shafiquzzaman, M., Murakami, S., Schneider, M.D., Mishina, Y., Li, B.J., and Li, J. (2018). BMPRIA is required for osteogenic differentiation and RANKL expression in adult bone marrow mesenchymal stromal cells. Sci Rep *8, 8475*.

Chen, H., Tan, X.N., Hu, S., Liu, R.Q., Peng, L.H., Li, Y.M., and Wu, P. (2021). Molecular Mechanisms of Chondrocyte Proliferation and Differentiation. Front Cell Dev Biol *9*, 664168.

Cox, T.C., Camci, E.D., Vora, S., Luquetti, D.V., and Turner, E.E. (2014). The genetics of auricular development and malformation: new findings in model systems driving future directions for microtia research. Eur J Med Genet *57*, 394-401.

DiDomenico, C.D., Lintz, M., and Bonassar, L.J. (2018). Molecular transport in articular cartilage - what have we learned from the past 50 years? Nat Rev Rheumatol *14*, 393-403.

Dy, P., Wang, W., Bhattaram, P., Wang, Q., Wang, L., Ballock, R.T., and Lefebvre, V. (2012). Sox9 directs hypertrophic maturation and blocks osteoblast differentiation of growth plate chondrocytes. Dev Cell *22*, 597-609.

Evenbratt, H., Andreasson, L., Bicknell, V., Brittberg, M., Mobini, R., and Simonsson, S. (2022). Insights into the present and future of cartilage regeneration and joint repair. Cell Regen *11*, 3.

Fuchs, J.C., and Tucker, A.S. (2015). Development and Integration of the Ear. Curr Top Dev Biol *115*, 213-232.

Ge, X.Z., Chen, Y.E., Song, D.Y., McDermott, M., Woyshner, K., Manousopoulou, A., Wang, N., Li, W., Wang, L.D., and Li, J.J. (2021). Clipper: P-value-free FDR control on high-throughput data from two conditions. Genome Biol *22*, 288.

Gendron, C., Schwentker, A., and van Aalst, J.A. (2016). Genetic Advances in the Understanding of Microtia. J Pediatr Genet *5*, 189-197.

Haseeb, A., Kc, R., Angelozzi, M., de Charleroy, C., Rux, D., Tower, R.J., Yao, L., Pellegrino da Silva, R., Pacifici, M., Qin, L*., et al.* (2021). SOX9 keeps growth plates and articular cartilage healthy by inhibiting chondrocyte dedifferentiation/osteoblastic redifferentiation. Proc Natl Acad Sci U S A *118*, e2019152118.

He, G., Shi, Y., Lim, J., Bellido, T., Ni, J., and Long, F. (2017). Differential involvement of Wnt signaling in Bmp regulation of cancellous versus periosteal bone growth. Bone Res *5*, 17016.

Horigome, Y., Ida-Yonemochi, H., Waguri, S., Shibata, S., Endo, N., and Komatsu, M. (2020). Loss of autophagy in chondrocytes causes severe growth retardation. Autophagy *16*, 501-511.

Huang, W., Zhou, X., Lefebvre, V., and de Crombrugghe, B. (2000). Phosphorylation of SOX9 by cyclic AMP-dependent protein kinase A enhances SOX9's ability to transactivate a Col2a1 chondrocyte-specific enhancer. Mol Cell Biol *20*, 4149-4158.

552 Huang, Y., Huang, X., Li, K., and Yang, Q. (2023). Risk Factors of Isolated Microtia: A Systematic
553 Review and Meta-Analysis. Plast Reconstr Surg *151*, 651e-663e.
554 Jing, Y., Jing, J., Ye, L., Liu, X., Harris, S.E., Hinton, R.J., and Feng, J.Q. (2017). Chondrogenesis and
555 osteogenesis are one continuous developmental and lineage defined biological process. Sci Rep
556 *7*, 10020.
557 Kobayashi, S., Takebe, T., Inui, M., Iwai, S., Kan, H., Zheng, Y.W., Maegawa, J., and Taniguchi, H.
558 (2011). Reconstruction of human elastic cartilage by a CD44+ CD90+ stem cell in the ear
559 perichondrium. Proc Natl Acad Sci U S A *108*, 14479-14484.
560 Kozhemyakina, E., Lassar, A.B., and Zelzer, E. (2015). A pathway to bone: signaling molecules and
561 transcription factors involved in chondrocyte development and maturation. Development *142*,
562 817-831.
563 Lefebvre, V., Angelozzi, M., and Haseeb, A. (2019). SOX9 in cartilage development and disease.
564 Curr Opin Cell Biol *61*, 39-47.
565 Lim, J., Shi, Y., Karner, C.M., Lee, S.Y., Lee, W.C., He, G., and Long, F. (2016). Dual function of Bmpr1a
566 signaling in restricting preosteoblast proliferation and stimulating osteoblast activity in mouse.
567 Development *143*, 339-347.
568 Liu, C.F., Samsa, W.E., Zhou, G., and Lefebvre, V. (2017). Transcriptional control of chondrocyte
569 specification and differentiation. Semin Cell Dev Biol *62*, 34-49.
570 Liu, H., Li, P., Zhang, S., Xiang, J., Yang, R., Liu, J., Shafiquzzaman, M., Biswas, S., Wei, Z., Zhang, Z.,
571 *et al.* (2022). Prrx1 marks stem cells for bone, white adipose tissue and dermis in adult mice. Nat
572 Genet *54*, 1946-1958.
573 Lu, M., Lu, X., Jiang, H., and Pan, B. (2020). Review of Preferential Suspicious Genes in Microtia
574 Patients Through Various Approaches. J Craniofac Surg *31*, 538-541.
575 Martin, J.F., Bradley, A., and Olson, E.N. (1995). The Paired-Like Homeo Box Gene Mhox Is Required
576 for Early Events of Skeletogenesis in Multiple Lineages. Gene Dev *9*, 1237-1249.
577 Mizuhashi, K., Ono, W., Matsushita, Y., Sakagami, N., Takahashi, A., Saunders, T.L., Nagasawa, T.,
578 Kronenberg, H.M., and Ono, N. (2018). Resting zone of the growth plate houses a unique class of
579 skeletal stem cells. Nature *563*, 254-258.
580 Morita, M., Yoneda, A., Tokunoh, N., Masaki, T., Shirakura, K., Kinoshita, M., Hashimoto, R.,
581 Shigesada, N., Takahashi, J., Tachibana, M., *et al.* (2023). Upregulation of Robo4 expression by
582 SMAD signaling suppresses vascular permeability and mortality in endotoxemia and COVID-19
583 models. Proc Natl Acad Sci U S A *120*, e2213317120.
584 Murtaugh, L.C., Chyung, J.H., and Lassar, A.B. (1999). Sonic hedgehog promotes somitic
585 chondrogenesis by altering the cellular response to BMP signaling. Genes Dev *13*, 225-237.
586 Newton, P.T., Li, L., Zhou, B., Schweingruber, C., Hovorakova, M., Xie, M., Sun, X., Sandhow, L.,
587 Artemov, A.V., Ivashkin, E., *et al.* (2019). A radical switch in clonality reveals a stem cell niche in the
588 epiphyseal growth plate. Nature *567*, 234-238.
589 Nordberg, R.C., Otarola, G.A., Wang, D., Hu, J.C., and Athanasiou, K.A. (2022). Navigating
590 regulatory pathways for translation of biologic cartilage repair products. Sci Transl Med *14*,
591 eabp8163.
592 Omi, M., Kaartinen, V., and Mishina, Y. (2019). Activin A receptor type 1-mediated BMP signaling
593 regulates RANKL-induced osteoclastogenesis via canonical SMAD-signaling pathway. J Biol Chem
594 *294*, 17818-17836.

595 Quiat, D., Kim, S.W., Zhang, Q., Morton, S.U., Pereira, A.C., DePalma, S.R., Willcox, J.A.L.,
596 McDonough, B., DeLaughter, D.M., Gorham, J.M., *et al.* (2022). An ancient founder mutation
597 located between ROBO1 and ROBO2 is responsible for increased microtia risk in Amerindigenous
598 populations. Proc Natl Acad Sci U S A *119*, e2203928119.
599 Retting, K.N., Song, B., Yoon, B.S., and Lyons, K.M. (2009). BMP canonical Smad signaling through
600 Smad1 and Smad5 is required for endochondral bone formation. Development *136*, 1093-1104.
601 Ritter, K.E., and Martin, D.M. (2019). Neural crest contributions to the ear: Implications for
602 congenital hearing disorders. Hear Res *376*, 22-32.
603 Siddappa, R., Martens, A., Doorn, J., Leusink, A., Olivo, C., Licht, R., van Rijn, L., Gaspar, C., Fodde,
604 R., Janssen, F., *et al.* (2008). cAMP/PKA pathway activation in human mesenchymal stem cells in
605 vitro results in robust bone formation in vivo. Proc Natl Acad Sci U S A *105*, 7281-7286.
606 Takarada, T., Hinoi, E., Nakazato, R., Ochi, H., Xu, C., Tsuchikane, A., Takeda, S., Karsenty, G., Abe,
607 T., Kiyonari, H., *et al.* (2013). An analysis of skeletal development in osteoblast-specific and
608 chondrocyte-specific runt-related transcription factor-2 (Runx2) knockout mice. J Bone Miner Res
609 *28*, 2064-2069.
610 ten Berge, D., Brouwer, A., Korving, J., Martin, J.F., and Meijlink, F. (1998). Prx1 and Prx2 in
611 skeletogenesis: roles in the craniofacial region, inner ear and limbs. Development *125*, 3831-3842.
612 Thielen, N.G.M., van der Kraan, P.M., and van Caam, A.P.M. (2019). TGFbeta/BMP Signaling
613 Pathway in Cartilage Homeostasis. Cells *8*, 969.
614 Tsang, K.Y., and Cheah, K.S. (2019). The extended chondrocyte lineage: implications for skeletal
615 homeostasis and disorders. Curr Opin Cell Biol *61*, 132-140.
616 Tumelty, K.E., Higginson-Scott, N., Fan, X., Bajaj, P., Knowlton, K.M., Shamashkin, M., Coyle, A.J., Lu,
617 W., and Berasi, S.P. (2018). Identification of direct negative cross-talk between the SLIT2 and bone
618 morphogenetic protein-Gremlin signaling pathways. J Biol Chem *293*, 3039-3055.
619 Ueharu, H., and Mishina, Y. (2023). BMP signaling during craniofacial development: new insights
620 into pathological mechanisms leading to craniofacial anomalies. Front Physiol *14*, 1170511.
621 Wang, C., Tan, Z.J., Niu, B., Tsang, K.Y., Tai, A., Chan, W.C.W., Lo, R.L.K., Leung, K.K.H., Dung, N.W.F.,
622 Itoh, N., *et al.* (2018). Inhibiting the integrated stress response pathway prevents aberrant
623 chondrocyte differentiation thereby alleviating chondrodysplasia. Elife *7*, e37673.
624 Wang, C.Y., Core, A.B., Canali, S., Zumbrennen-Bullough, K.B., Ozer, S., Umans, L., Zwijsen, A., and
625 Babitt, J.L. (2017). Smad1/5 is required for erythropoietin-mediated suppression of hepcidin in
626 mice. Blood *130*, 73-83.
627 Xie, Y., Zinkle, A., Chen, L., and Mohammadi, M. (2020). Fibroblast growth factor signalling in
628 osteoarthritis and cartilage repair. Nat Rev Rheumatol *16*, 547-564.
629 Yang, G., Zhu, L., Hou, N., Lan, Y., Wu, X.M., Zhou, B., Teng, Y., and Yang, X. (2014a). Osteogenic
630 fate of hypertrophic chondrocytes. Cell Res *24*, 1266-1269.
631 Yang, L., Tsang, K.Y., Tang, H.C., Chan, D., and Cheah, K.S. (2014b). Hypertrophic chondrocytes can
632 become osteoblasts and osteocytes in endochondral bone formation. Proc Natl Acad Sci U S A
633 *111*, 12097-12102.
634 Yoon, B.S., Ovchinnikov, D.A., Yoshii, I., Mishina, Y., Behringer, R.R., and Lyons, K.M. (2005). Bmpr1a
635 and Bmpr1b have overlapping functions and are essential for chondrogenesis in vivo. Proc Natl
636 Acad Sci U S A *102*, 5062-5067.
637 Yoon, B.S., Pogue, R., Ovchinnikov, D.A., Yoshii, I., Mishina, Y., Behringer, R.R., and Lyons, K.M.

(2006). BMPs regulate multiple aspects of growth-plate chondrogenesis through opposing actions on FGF pathways. Development *133*, 4667-4678.

Zhang, H., Zhang, Y., Terajima, M., Romanowicz, G., Liu, Y., Omi, M., Bigelow, E., Joiner, D.M., Waldorff, E.I., Zhu, P.*, et al.* (2020). Loss of BMP signaling mediated by BMPR1A in osteoblasts leads to differential bone phenotypes in mice depending on anatomical location of the bones. Bone *137*, 115402.

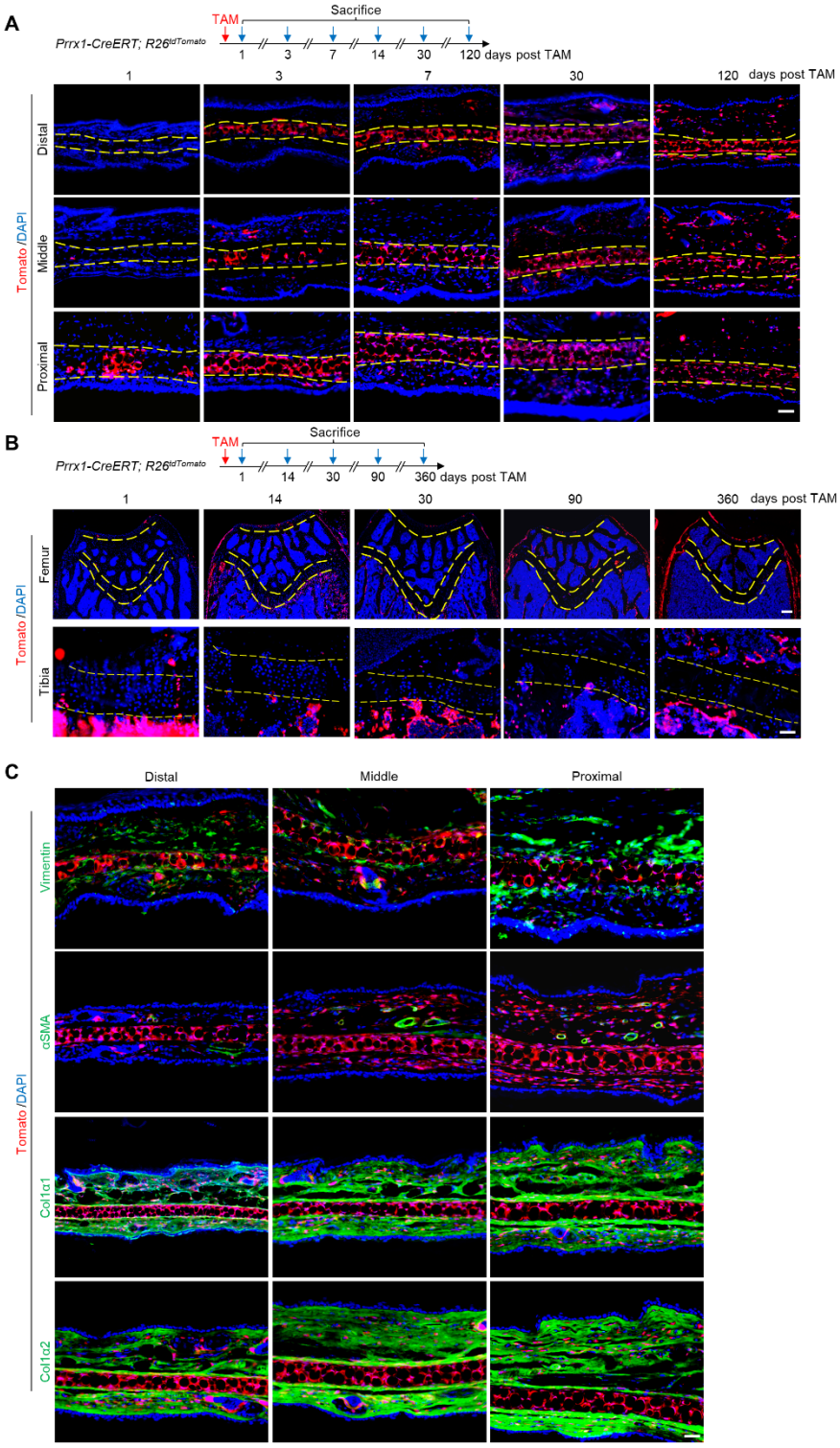

Figure 1

Figure 1. *Prrx1* marks auricle chondrocytes but few epiphyseal or articular chondrocytes.

A. Genetic tracing experiments showed that *Prrx1* marks all chondrocytes in the auricle. Upper panel: a diagram showing the schedule for TAM administration and mouse euthanasia. Scale bars=50 μm.

B. Genetic tracing experiments showed that *Prrx1* marks few cells in the articular cartilage or the growth plates of femurs and the growth plates of tibias in adult mice. Scale bars (femur)=100 μm. Scale bars (tibia)=50 μm.

C. Representative immunostaining results for Vimentin, αSMA, Col1α1, and Col1α2 in ear sections of *Prrx1-CreERT; R26*^{tdTomato} mice. Scale bars=50 μm.

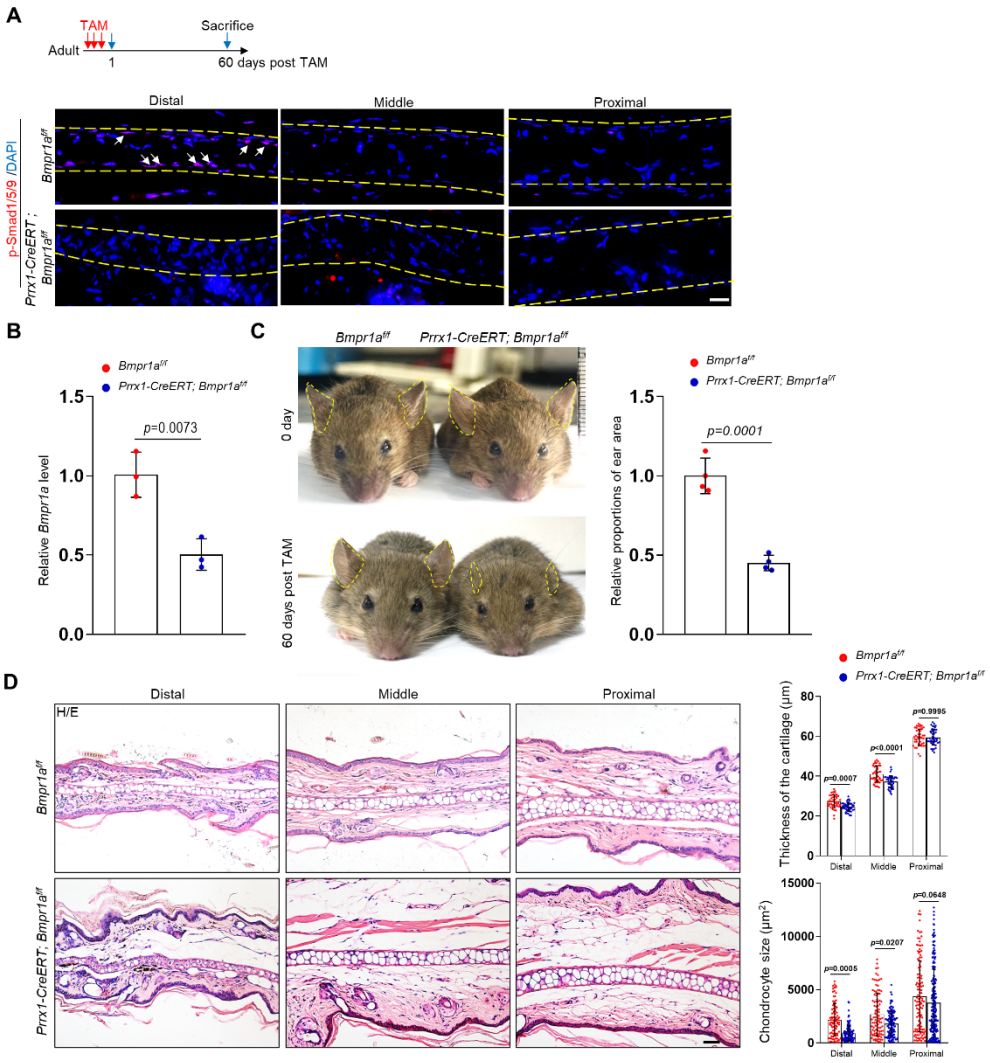

Figure 2

Figure 2. Ablation of *Bmpr1a* in *Prrx1*$^{+}$ cells in adult mice led to microtia.

A. A decrease in p-Smad1/5/9 on the ear sections of the *Prrx1-CreERT; Bmpr1a*$^{f/f}$ mice. Upper panel: Schedule for TAM administration and mouse euthanasia. Scale bars=20 μm. Arrows: positive signals. Smad1/5/9 staining results.

B. qPCR analysis of *Bmpr1a* mRNA in the ear samples of the *Prrx1-CreERT; Bmpr1a*$^{f/f}$ and control mice. N=3.

C. The ear phenotypes of the *Prrx1-CreERT; Bmpr1a*$^{f/f}$ mice 2 months after TAM administration to adult male mice. Right panel: quantitation data. N=4.

D. H/E staining of ear sections from the mutant and control mice. Right panels: The thickness of the cartilage and the size of the chondrocytes in the ears of the mutant and control mice. Scale bars=50 μm. N=3. Unpaired two-tailed Student's t test were applied to evaluate the correlation data in (B and C). Two-way ANOVA (or mixed model) multiple comparisons were applied to evaluate the correlation data in (D), $p<0.05$ was considered as statistically significant.

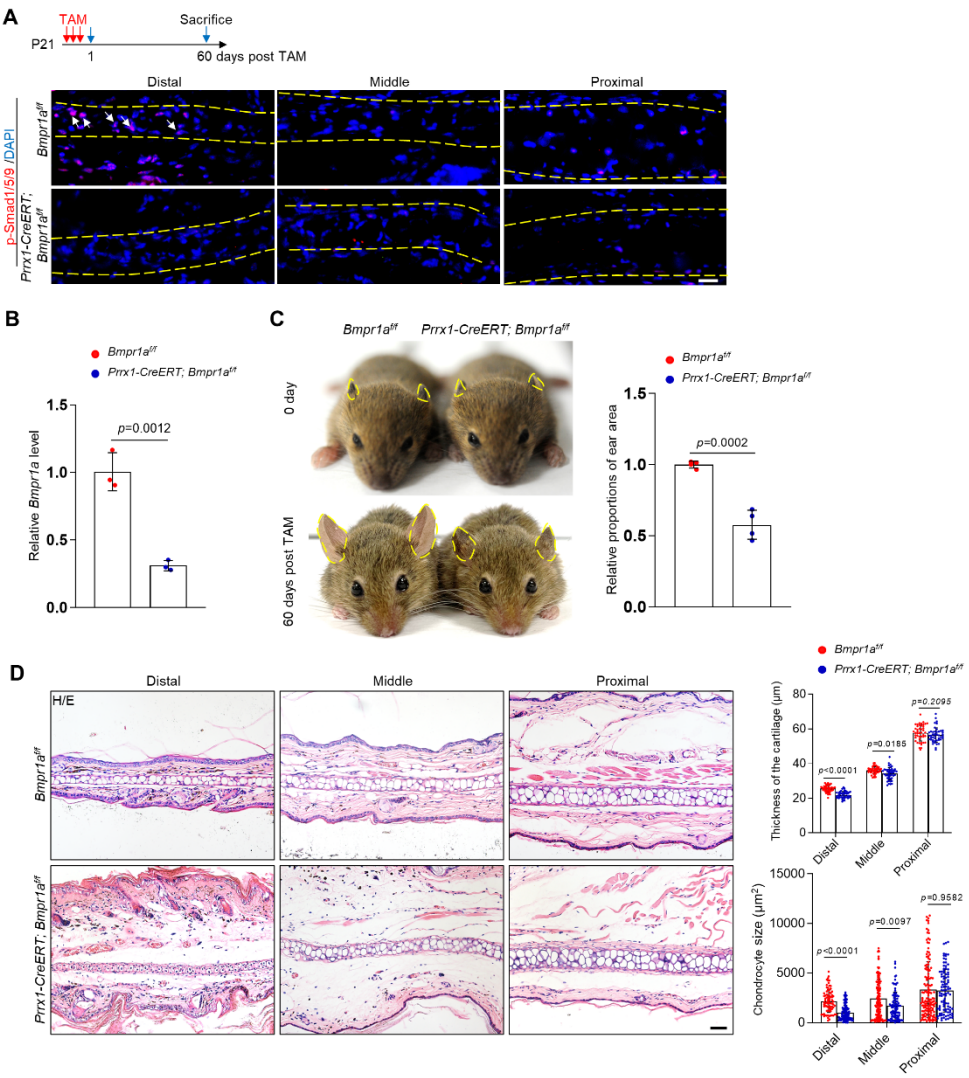

Figure 3

Figure 3. Ablation of *Bmpr1a* in *Prrx1*$^{+}$ cells in young mice led to microtia.

A. A decrease in p-Smad1/5/9 on the ear sections of the *Prrx1-CreERT; Bmpr1a*$^{f/f}$ mice that received TAM at P21. Upper panel: Schedule for TAM administration and mouse euthanasia. Scale bars=20 μm. Arrows: positive signals.

B. qPCR analysis of *Bmpr1a* mRNA in the ear samples of the *Prrx1-CreERT; Bmpr1a*$^{f/f}$ and control mice. N=3.

C. The ear phenotypes of the adult *Prrx1-CreERT; Bmpr1a*$^{f/f}$ mice that received Tam at P21. Right panel: quantitation data. N=4.

D. H/E staining of ear sections from the mutant and control mice. Right panels: The thickness of the cartilage and the size of the chondrocytes in the ears of the mutant and control mice. Scale bars=50 μm. N=3. Unpaired two-tailed Student's t test were applied to evaluate the correlation data in (B and C). Two-way ANOVA (or mixed model) multiple comparisons were applied to evaluate the correlation data in (D), $p<0.05$ was considered as statistically significant.

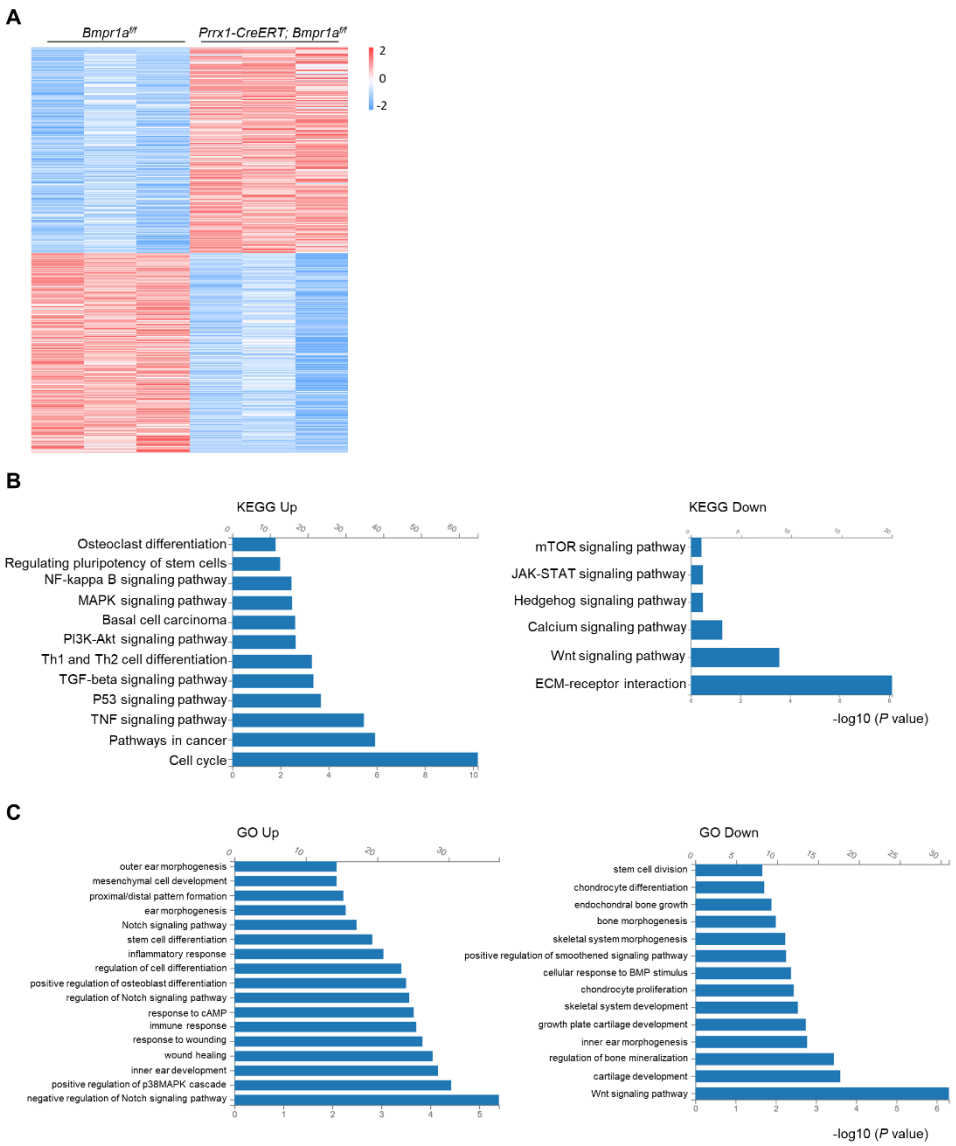

Figure 4

Figure 4. Alteration of transcription profiles in *Bmpr1a*-deficient chondrocytes.
A. Heatmaps of the top 500 genes expressed in the distal part of the auricle of the *Prrx1-CreERT; Bmpr1a*$^{f/f}$ and age- and gender-matched control mice. N=3.
B. KEGG analysis results of the pathways affected by *Bmpr1a* ablation.
C. GO analysis results of the modules affected by *Bmpr1a* ablation.

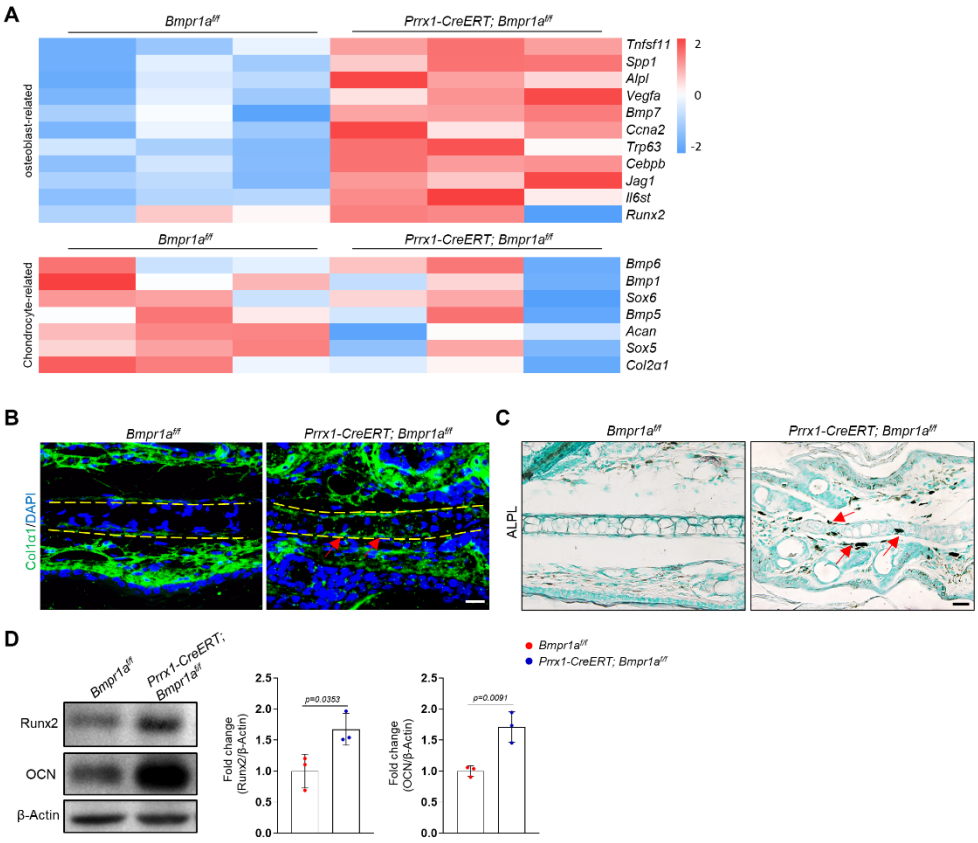

Figure 5

Figure 5. *Bmpr1a* deficiency leads to an auricle chondrocyte fate switch to osteoblasts.

A. Heatmaps of osteoblast-related genes and chondrocyte-related genes differentially expressed in the *Bmpr1a*-deficient and control mice. N=3.

B. Immunostaining results for Col1α1 in ear sections of the *Bmpr1a*-deficient and control mice. Scale bars=20 μm. Arrows: positive signals.

C. ALP activity was greatly increased in the auricle of the *Prrx1-CreERT; Bmpr1a*$^{f/f}$ mice compared to the control mice. Scale bars=50 μm. Arrows: positive signals.

D. WB results showed that the expression of the osteoblast marker genes Runx2 and osteocalcin was increased in the mutant samples. Right panel: quantitation data. N=3. Unpaired two-tailed Student's t test were applied to evaluate the correlation data in (D), $p<0.05$ was considered as statistically significant.

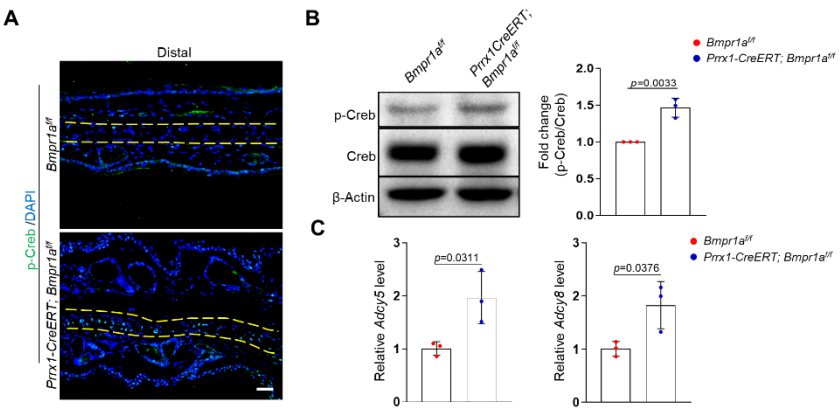

Figure 6

Figure 6. *Bmpr1a* deficiency led to hyperactivation of PKA signaling.

A. Immunoassaying for p-Creb in the ear sections of the *Bmpr1a*-deficient and control mice.

B. Western blot analysis of p-Creb in auricle samples of the *Bmpr1a*-deficient and control mice. Right panel: quantitation data. N=3.

C. qPCR results for *Adcy5* and *Adcy8* in auricle samples of the *Bmpr1a*-deficient and control mice. N=3. Unpaired two-tailed Student's t test were applied to evaluate the correlation data in (B and C), $p<0.05$ was considered as statistically significant.

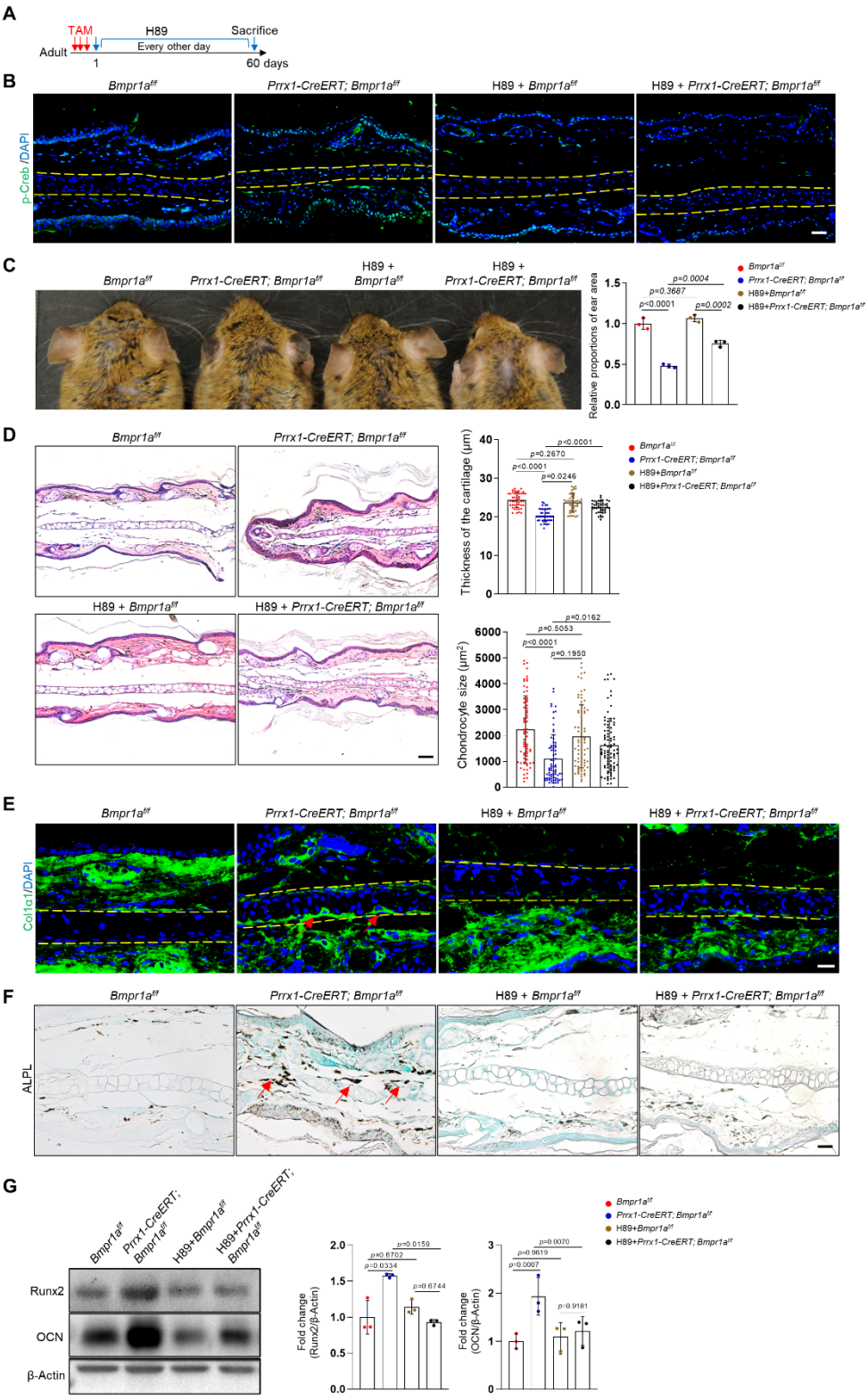

Figure 7

Figure 7. Inhibition of PKA signaling blocks microtia development in *Bmpr1a*-deficient mice

A. Diagram showing the schedule of TAM and H89 administration.

B. Immunostaining results of p-Creb in ear sections of the H89-treated mutant and control mice. Scale bars=50 μm.

C. The rescue of the microtia phenotype in the mutant mice by H89. Right panels: Quantitation data. N=3.

D. H/E staining results. Right panels: the thickness of the cartilage and the size of the chondrocytes in the ear of the mutant and control mice. N=3. Right panels: Quantitation data. Scale bars=50 μm. N=3.

E. Immunostaining results for Col1α1 in the ear sections of the H89-treated mutant and control mice. Scale bars=20 μm. Arrows: positive signals.

F. ALP activity was greatly suppressed by H89 in the auricle of the *Prrx1-CreERT; Bmpr1a*$^{f/f}$ mice compared to the control mice. Scale bars=50 μm. Arrows: positive signals.

G. WB blot also showed that H89 rescued the expression of the osteoblast marker genes Runx2 and osteocalcin in the mutant mice. Right panel: quantitation data. N=3. One-way ANOVA (and nonparametric or mixed) multiple comparisons were applied to evaluate the correlation data in (C, D, and G). $p<0.05$ was considered as statistically significant.